Unsteady Heat Transfer Coefficient Estimation for Long Duration

James K. Hodge* and Alice J. Chen†
Air Force Institute of Technology, Wright-Patterson Air Force Base, Ohio
and
James R. Hayes‡
Air Force Wright Aeronautical Laboratories, Wright-Patterson Air Force Base, Ohio

Measurement of convective heat rate is difficult in ground and flight tests due to thermal and chemical mismatches between gages and surface materials. Coaxial thermocouple gages, which can be matched with metallic surfaces, are attractive if the data reduction problem can be solved. A one-dimensional estimation algorithm with a Kalman filter is extended for coaxial gages with surface and backface temperature measurements. The algorithm estimates parameters for changes in the heat-transfer coefficient due to pitch sweep and other time variations, for specific heat capacity and conductivity, and for effective gage length. Results of a hypersonic wind-tunnel test for a blunt plate with an imbedded Teflon button are compared with numerical solutions of the Navier-Stokes and boundary-layer equations.

Nomenclature

a,b = heat equation coefficients
A = tridiagonal coefficient matrix
$\bar{B}, \bar{D}$ = dummy vectors
c = specific heat
c_k,d = dummy constants
h = heat-transfer coefficient
G = Kalman filter gain matrix
H = binary thermocouple location matrix
I = identity matrix or maximum index for spatial nodes
j = index for arbitrary time segments
J = conditional information matrix
K = conductivity
L = reference length or plate length
$\bar{L}'$ = gradient of likelihood function
p = static pressure
P = covariance matrix
q = convective heating flux
Q = total heating load
Q' = heating error covariance matrix
R = measurement covariance matrix
Re = Reynolds number based on reference length
s = curvilinear distance along surface
$\bar{S}_k$ = sensitivity of temperature to kth parameter
St = Stanton number
t = time
T_{aw} = adiabatic wall temperature
$\bar{U}$ = material temperature at nodes
x = spatial depth from gage surface
$\bar{Y}$ = thermocouple measurement vector
α = thermal diffusivity
ϕ = thermal parameter factors (ideally $\phi = 1$)
Φ = transition matrix
μ = step function with linear ramp
θ = vector of estimation parameters
δ = deflection angle or angle of attack

Superscripts
(s) = iteration index
0 = initial value at each time segment
$+$ = updated or a posteriori value

Subscripts
i = index for node location
k = estimation parameter index
m,n = time level index or sampling index
o = stagnation condition
∞ = freestream condition

Introduction

MOST convective heat flux measurements in ground tests are only of short duration. Although this may be due to facility limitations, it is usually due to gage or data reduction limitations. If the test time could be increased, then overall test time and cost could be decreased by using transient test techniques (such as sweeps in angle of attack, sideslip, and control surface deflection). Although the time duration can be controlled in a ground test, it often cannot be in a flight test, which is usually of very long duration. Even when gages are installed properly, the long-duration tests lead to errors in heat flux primarily due to three effects.

First, a heat flux gage is usually made of a different material than the model or vehicle and has a different transient thermal response. A decrease (or increase) in wall temperature between the gage and the surrounding material (a thermal mismatch that can be approximated by a discontinuous step in wall temperature) becomes larger with time, and then decreases if thermal equilibrium is approached. This can cause a time varying error in the heat-transfer coefficient[1,2] if the difference between the adiabatic wall temperature and the wall temperature is not significantly larger than the wall temperature step. The gage may accurately measure the heat flux to the gage, but not the heat flux to the surrounding surface, which is needed.

A second effect can cause errors if dissociated species are present, especially for a hypersonic vehicle with a small nose radius at high altitude. The different gage material or coating could be different catalytically than the vehicle (i.e., different rates of recombination of dissociated species).[3,4] This chemical nonequilibrium effect can cause a step change in wall enthalpy and thus heat flux.

Third, an additional error in convective heat flux is caused by heat conduction tangential to the surface. This can be due to spatial gradients in wall temperature, such as the gradients

Presented as Paper 86-1240 at the AIAA/ASME 4th Joint Thermophysics and Heat Transfer Conference, Boston, MA, June 2-4, 1986; received Nov. 11, 1986; revision received June 29, 1987.

*Major, U.S. Air Force, Associate Professor of Aeronautics and Astronautics.
†Captain, U.S. Air Force, Graduate Student.
‡Aerospace Engineer.

caused by the thermal and chemical mismatches just described. If the gage is very small such that thermal equilibrium in the materials is reached very rapidly, then the error (or lag) may be insignificant, although the response time is limited.

Coaxial thermocouple gages can be used to minimize some of the described effects for a metallic surface[5-8] but require data reduction algorithms. Since coaxial gages can be made of metallic materials (such as copper, constantan, chromel, alumel, and platinum-rhodium), it is possible for gages to be matched thermally and chemically. The thermocouple junction at the surface can be formed by a vacuum-deposited metallic plating of 1-μm thickness to provide a very fast response time or gages on curved surfaces can be contoured and the junction formed by sanding. The gage diameter can be as small as 0.05 mm, and long in length if a semi-infinite slab assumption is used for data reduction.[5-7,9] An additional thermocouple junction at the back of the gage provides a backface temperature measurement for numerical data reduction algorithms.[7] Thus, the need for a long gage can be eliminated and account made for the heat loss at the back of the gage. Numerical data reduction problems will be addressed further in this article.

A one-dimensional estimation algorithm,[10,11] which was used to reduce Space Shuttle thermocouple data and requires no smoothing of input thermocouple measurements, is modified for the coaxial gage and extended. The specific heat, conductivity, and effective length of the gage are computed as fixed parameters. In addition to original capabilities of estimating a constant heat coefficient and the heat coefficient as a linear spline in deflection angle as fixed parameters over all data samples or over selected time segments, time variations in the heat-transfer coefficient are separately correlated from variations due to time variation of the deflection angle. Another new option allows computation of a time history for the heat-transfer coefficient with no correlation by conditioning estimates at each time step by any combination of past, present, and future measurements.

Major objectives of this article are to demonstrate some of the unique capabilities of the new estimation algorithm and to reduce some coaxial thermocouple data with variations in heat-transfer coefficient due to deflection angle and with time variations in the coefficient due to a thermal mismatch. To accomplish these objectives, temperature measurements are first simulated with a known heat-transfer coefficient and other parameters for two check cases. The first case is for a gage of semi-infinite length, and the second is for a gage of finite length. Results from three inverse algorithms are compared with results from the estimation algorithm. Uncertainty and time variations (though perhaps small) in actual wind-tunnel tests are avoided. Second, actual data from a coaxial gage imbedded in a Teflon button on a steel plate during a hypersonic wind-tunnel test are reduced to demonstrate time variations in the heat-transfer coefficient caused by a thermal mismatch in addition to variations due to deflection angle. Finally, computational solutions of the Navier-Stokes and boundary-layer equations are compared with the experimental results with a thermal mismatch.

Data Reduction Algorithms

Four different data reduction algorithms for a coaxial gage are compared. The first algorithm is based on an analytical solution for heat flux and will be referred to as an "analytical inverse" method. The second is in terms of integrated heat load and will be referred to as an "integral inverse" method. The third is based on an explicit numerical solution of the heat equation and is referred to as a "numerical inverse" method. The fourth and new algorithm is based on stochastic estimation theory with a Kalman filter as an integral part, and on implicit numerical solutions of the heat equation. The new algorithm is referred to as an "estimation" method. A summary of each follows.

Inverse Algorithms

The analytical inverse method is used widely for data reduction for thin film and coaxial gages.[9] It is based on integration of the heat equation assuming a one-dimensional semi-infinite slab with constant thermal properties and a surface temperature time history described by continuous linear spline fits. The solution is given by

$$\dot{q}(t_n) = 2\sqrt{\rho cK/\pi} \sum_{m=1}^{n} \frac{[Y_1(t_m) - Y_1(t_{m-1})]}{\sqrt{t_n - t_m} + \sqrt{t_n - t_{m-1}}} \tag{1}$$

where only the surface temperature measurement Y_1 is used. Since the temperature measurement is assumed to be at the surface, this is not an "illposed" inverse method.[12] However, the method is sensitive to noise. Therefore, some smoothing or filtering of the measurement time history is needed, but this usually causes gain loss and lag for a transient signal.

Another integral inverse method is used sometimes in an attempt to smooth the data.[13] The integral solution of the heat equation with the given assumptions is given by

$$Q(t_n) = \sqrt{\rho cK/\pi} \sum_{m=1}^{n} \frac{[Y_1(t_m) - Y_1(t_{m-1})]\,\Delta t}{\sqrt{t_n - t_m} + \sqrt{t_n - t_{m-1}}} \tag{2a}$$

This heat load must be differentiated then by a difference equation such as

$$\dot{q}(t_n) = [-2Q0(t_{n-8}) - Q(t_{n-4}) + Q(t_{n+4}) + 2Q(t_{n+8})]/40\Delta t \tag{2b}$$

but still needs smooth measurements. It is also limited by the semi-infinite slab assumption.

A numerical inverse method avoids the semi-infinite slab assumption and can account for heat loss at the back of the gage when a backface measurement is provided.[9] Such an algorithm, based on an explicit difference solution of the heat equation, is given for equally spaced nodes by

$$a[U_i(t_{n+1}) - U_i(t_n)] = b[U_{i-1}(t_n) - 2U_i(t_n) + U_{i+1}(t_n)] \tag{3a}$$

$$q(t_n) = -b[-3Y_1(t_n) + 4U_2(t_n) - U_3(t_n)]/2 \tag{3b}$$

where $a = \rho c\Delta x/\Delta t$ and $b = K/\Delta x$. The measurements are used directly at discrete nodes and need to be smoothed. This algorithm also has a stability constraint on the time step, which often requires interpolation between measurements. An implicit method would remove the constraint but would still be sensitive to noise. An implicit method is available instead in an estimation method.[10]

Estimation Algorithm

The estimation algorithm consists of three major but integral parts. First, the temperature, the sensitivity to each parameter, and the covariance of the temperature are predicted numerically at each spatial node. Second, the predictions are updated by a Kalman filter, which handles noisy data properly. Finally, a Newton-Raphson algorithm iterates for appropriate parameters at the end of arbitrarily selected time segments or at each sample. Since options available in the algorithm are numerous, only extensions and unique aspects as applied to coaxial gages are emphasized.

To predict the temperature, an energy balance for one-dimensional finite elements is written at the surface and interior nodes as

$$a[U_1(t_n) - U_1(t_{n-1}^+)]/2 = b[U_2(t_n) - U_1(t_n)] + h(t_n,\delta_n)\,[T_{aw} - U_1(t_n)] \tag{4a}$$

$$a[U_i(t_n) - U_i(t^+_{n-1})] = b[U_{i-1}(t_n) - 2U_i(t_n) + U_{i+1}(t_n)]$$
$$\text{for } i = 2,3,\ldots I-1 \quad (4b)$$

$$a[U_I(t_n) - U_I(t^+_{n-1})] = b[U_{I-1}(t_n) - U_I(t_n)] \quad (4c)$$

where $a = \phi_c c \phi_x \Delta x/\Delta t$ and $b = \phi_k K/\phi_x \Delta x$. For simplicity, a negligible radiation term has been left out, and the spatial node step size is constant in Eq. (4), but not in the algorithm. Note that an equation at the surface [Eq. (4a)] is given and that the temperature measurements (Y) are not used. Equations (4) can be rewritten as a tridiagonal matrix equation of the form

$$\dot{\bar{U}} = [A - Z]\bar{U} + \bar{B} \quad (4d)$$

where $\bar{B} = 0$ except for $B_1 = hT_{aw}/a$, and $Z = 0$ except for $Z_{11} = h/a$. The tridiagonal matrix A is symmetric and constant for constant properties and an isothermal wall. Equations (4) are solved easily by a tridiagonal solution algorithm when all parameters have been prescribed or initialized.

Both thermal and heat-transfer parameters are guessed and later computed by iteration. Of primary interest is the heat-transfer coefficient defined by

$$h[t_n, \delta(t_n)] = q(t_n)/[T_{aw} - U_1(t_n^+)] \quad (5)$$

where $T_{aw} = 0.9T_o(t_n)$ is assumed for hypersonic flow. Theoretically, h is not a function of time for an isothermal wall and is thus nearly constant in short-duration wind-tunnel tests. However, for long-duration tests and for pitch sweeps, the coefficients of linear spline fits in time and deflection angle are chosen as parameters. The spline fits are defined as follows:

$$h = \begin{cases} h_0 + h_t(t_n - t_0) + h_{\delta 1}(\delta - \delta_0) & \text{for } \delta < \delta_1 \\ h_0 + h_t(t_n - t_0) + h_{\delta 1}(\delta_1 - \delta_0) & \\ \quad + h_{\delta 2}(\delta - \delta_1) & \text{for } \delta_1 < \delta_2 \text{ etc.} \\ h_0 + h_t(t_n - t_0) + h_{\delta 1}(\delta_1 - \delta_0) & \\ \quad + h_{\delta 2}(\delta_2 - \delta_1) + \ldots & \\ \quad + h_{\delta 9}(\delta - \delta_8) & \text{for } \delta \le \delta_8 \end{cases} \quad (6)$$

The coefficients of the given spline fit (also linear slopes or partials) are prescribed or determined for each appropriate time range or segment. For example, Eq. (6) may be applied once over the time range of all measurements. As another example, Eq. (6) may be applied only between each measurement (in which case the parameters for slopes must be prescribed). In addition, factors for specific heat ϕ_c, conductivity ϕ_k, and effective gage length ϕ_x are prescribed or estimated. The parameter vector for the estimation algorithm is defined as

$$\bar{\theta} = \left[\phi_c\ \phi_k\ \phi_x\ h_0\ h_t\ h_{\delta 1}\ h_{\delta 2}\ \ldots\ h_{\delta 9}\right]^T \quad (7)$$

Equations for the sensitivity of the temperature to each of the parameters are obtained by differentiating Eqs. (4) with respect to $\bar{\theta}$. Equations for each of the k parameters are of the form

$$\dot{\bar{S}}_k = (A - Z)\bar{S}_k + c_k A\bar{U} + \bar{D}_k \quad (8)$$

where $c_k = 0$ except for $c_1 = 1/\phi_c$, $c_2 = 1/\phi_K$, and $c_3 = -2/\phi_x$; where

$$\bar{D} = 0 \text{ except for } D_1 = -h[T_{aw} - U_1(t_n)]a/\phi_c$$
$$- 2h[T_{aw} - U_1(t_n)]/a/\phi_k$$
$$h[T_{aw} - U_1(t_n)]/a\phi_x$$
$$[T_{aw} - U_1(t_n)]/a$$
$$(t_n - t_0)[T_{aw} - U(t_n)]/a$$
$$\mu(\delta)[T_{aw} - U_1(t_n)]/a \ \ldots$$
$$\mu(\delta)[T_{aw} - U_1(t_n)]/a \text{ for } k = 1,2,\ldots 14$$

The step function with a linear ramp is defined by

$$\mu(\delta) = \begin{cases} 0 & \text{for } \delta \le \delta_{k-6} \\ \delta - \delta_{k-6} & \text{for } \delta_{k-6} < \delta \le \delta_{k-5} \\ \delta_{k-5} - \delta_{k-6} & \text{for } \delta > \delta_{k-5} \end{cases}$$

Equation (8) for the sensitivity of each parameter is solved easily by a tridiagonal solution algorithm and the results used by the Kalman filter and the Newton-Raphson algorithm.

The covariance of Eqs. (4) with an exponential difference approximation gives an equation for the covariance matrix of the temperature given by[10]

$$P(t_n) = \Phi(\Delta t)P(t^+_{n-1})\Phi^T(\Delta t) + \int_0^{\Delta t} \Phi(\lambda)Q'\Phi^T(\lambda)d\lambda \quad (9)$$

The transition matrix Φ and integral in Eq. (9) are not easily computed, and a special decomposition of $(A-Z)$ (a tridiagonal, diagonally dominant, and nearly symmetric matrix) provides an approximate solution[10,14] that reduces computer time by an order of magnitude for 12 nodes compared to Taylor series methods (and even more for more nodes). If $(A-Z)$ is (or is assumed) constant, another reduction of four is obtained. The covariance matrix computed using Eq. (9) is needed by both the Kalman filter and the Newton-Raphson algorithm.

When predictions for the temperature, sensitivities, and covariance matrix are available (and temperature measurements are available at that time), an optimal Kalman filter[8,10,11,15] updates each according to the following equations:

$$\bar{U}(t_n^+) = \bar{U}(t_n) + G(t_n)[\bar{Y}(t_n) - H\bar{U}(t_n)] \quad (10)$$

$$\bar{S}_k(t_n^+) = [I - G(t_n)H]\ \bar{S}_k(t_n) \quad (11)$$

$$P(t_n^+) = [I - G(t_n)H]\ P(t_n)\ [I - G(t_n)H]^T + G(t_n)RG(t_n)^T \quad (12)$$

where

$$G(t_n) = P(t_n)\ H^T[HP(t_n)H^T + R]^{-1}H$$

After the updates are completed over a selected time segment, a modified Newton-Raphson iteration for that segment updates each parameter. The algorithm is given by

$$\bar{\theta}^{(s+1)} = \bar{\theta}^{(s)} + J^{-1}\bar{L}' \quad (13a)$$

where a conditional information matrix J approximates the Jacobian and a scoring technique approximates the gradient of the likelihood function. The components are approximated by

$$J_{k\ell} = \sum_{m=j1}^{j2} \bar{S}_k H^T[HP(t_m)H^T + R]^{-1}H\bar{S}_\ell(t_m) \quad (13b)$$

$$L_k' = \sum_{m=j1}^{j2} \bar{S}_k H^T [HP(t_m)H^T + R]^{-1} [\bar{Y}(t_m) - H\bar{U}(t_m)] \quad (13c)$$

where m refers to the sampling time t_m and j_1 and j_2 vary depending on which past, present, and/or future measurements are chosen. Previously, only temperature measurements within a prescribed time segment (i.e., time interval) were used.[10] However, the summations in Eqs. (13b) and (13c) can be changed, and a Gaussian-type weighting factor as a function of $(t_n - t_m)$ could be included. Three options or variations in j_1 and j_2 are emphasized for results in this article and are summarized as follows:

1) One time segment of all temperature measurements ($j_1 = 1$ and j_2 = total number of samples),

2) multiple but consecutive time segments over a limited number of measurements and time range (j_1 = index of first measurement in each time segment or interval and j_2 = index of last measurement), and

3) a new time segment is started after each new temperature measurement at t_n ($j_1 = n - 8$ and $j_2 = n + 8$).

Note that option 1 is appropriate for obtaining fixed thermal parameters such as factors of specific heat, conductivity, and effective gage length. Option 1 is also appropriate to obtain single best values for h_0, h_t, and h_δ. Option 2 is very appropriate when the time of discrete events is known (such as model injection into a wind tunnel or the beginning of a pitch sweep). Option 2 is also appropriate to obtain a time series of variations in parameters from which a general variation in the heat-transfer coefficient is obtained. Option 3 is new and only the parameter h_0 is computed (i.e., $h = h_0$); thus, only a time history for $h = h_0$ is obtained. With these options, both thermal and heat-transfer parameters are estimated, depending on the application.

Results

The estimation algorithm will first be demonstrated using option 1 for two check cases. The check cases consist of simulated measurements for a semi-infinite coaxial gage and then for a finite coaxial gage. Since these cases have known results and the assumed heat-transfer coefficient does not vary in time, the results of the estimation algorithm can be compared to three inverse algorithms. Then, experimental measurements for a coaxial gage imbedded in a Teflon button on a steel plate are analyzed to demonstrate the other options in the estimation algorithm when the heat-transfer coefficient is varying in time due to both changing deflection angle and a thermal mismatch. Since the correct results are not known, comparisons with computational solutions of the Navier-Stokes and boundary-layer equations for a prescribed thermal mismatch are presented.

Check Cases

The first check case is based on an exact analytical solution given by Eq. (1) for a semi-infinite slab (or very long coaxial gage). The surface temperature is first specified as a linear function in time and the heat-transfer coefficient as a step function to constant magnitude. A function for the adiabatic wall temperature (and thus stagnation temperature, assuming $T_{aw} = 0.9T_o$) is dictated then for a semi-infinite slab by Eq. (1). Surface and stagnation temperature measurements are then simulated according to these functions by sampling at a constant rate of 25 samples per second.

Results of the estimation and inverse algorithms for the first check case are shown in Figure 1. As expected, the analytical inverse algorithm gave exact values for h except for round-off error since the simulation was based on the analytical solution. Thus the ratio of h to the actual value of h is 1 as shown in Fig. 1. Since the integral inverse algorithm smooths over a range of eight past and future samples, low values are obtained initially at the step, as shown in Fig. 1. The numerical inverse algorithm obtained even lower values of h for the first samples

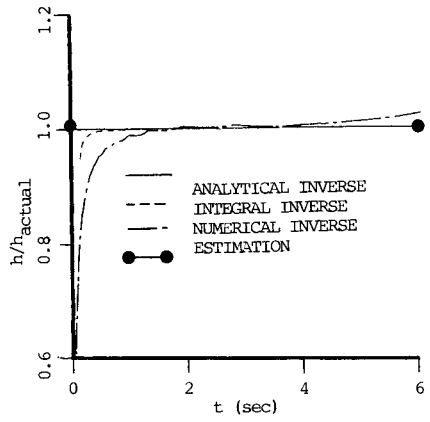

Fig. 1 Algorithm comparison using data simulated analytically for semi-infinite slab.

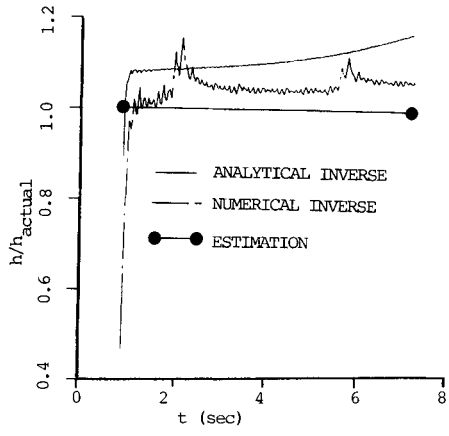

Fig. 2 Algorithm comparison using data simulated numerically for finite gage length.

as shown due to numerical truncation error and higher values at later times due to the assumption of a finite gage length for numerical purposes. The same assumption is necessary for the estimation algorithm. If only h_0 (i.e., constant h) is estimated using option 1, then three-decimal accuracy is obtained as shown. The estimation algorithm compensates for the truncation error at the step based on future measurements and obtains a "best" fit with data. If both the h_0 and h_t parameters are estimated using option 1, then h_0 is higher by a couple of percent, and h has a small negative slope and decreases to the correct value as shown. This is due to the numerical truncation error of the implicit method, which has the opposite sign from the explicit method. Results with options 2 and 3 are not shown but are similar except for a small oscillation starting at the step. The magnitude of the oscillation is dependent on the error matrix Q' and the measurement covariance R. The objective of most heat-transfer testing in wind tunnels is to obtain a best correlated and constant value of h, which the estimation algorithm accomplishes without the semi-infinite slab assumption.

For the second case, temperature measurements are simulated at the surface and backface of a finite gage of 12.8-mm length using the implicit numerical method in Eqs. (4). Data are sampled at unequal time intervals corresponding to realistic data with missing samples (referred to as data gaps). Results using the analytical inverse method are shown in Fig. 2. They are high initially because of the truncation error inherent in the simulated data, but increase in time due to the semi-infinite slab assumption of the reduction method. Results are not shown for the integral inverse algorithm since the algorithm was not designed for unequal steps. Results

from the numerical inverse algorithm are noisy as shown due to the variable time steps, although the method is valid for variable steps since it is only first-order accurate (results were considerably better for equal time steps). Results using the estimation algorithm with option 1 for h_0 and h_t are almost exact. The parameters are within six-decimal accuracy, and the ratio of h to the actual simulated h is shown in Fig. 2. Such excellent agreement is not surprising since the same truncation error is inherent in both the simulated data and the algorithm, but if the data is distorted randomly with white noise, the results are still as good, since the estimation algorithm is especially designed for noisy data.

Several other unique extensions[11] of the estimation algorithm were applied to the simulated data for a finite gage, and only results are discussed. Initial conditions were perturbed and estimated. An initial condition compatible with the measurements was estimated which minimized error in parameter estimates, but the estimated initial conditions were not unique. In another extension, any *one* of the thermal parameters (δ_c, ϕ_K, ϕ_x) were estimated to six-decimal accuracy simultaneously with h_0 using option 1. More than one thermal parameter and the heat coefficient cannot be estimated [this is an identifiability problem anticipated by multiplying Eq. (4a) by any constant]. If the heat-transfer coefficient is prescribed, then both the specific heat and conductivity can be estimated to six decimals. The estimation algorithm can therefore be used to determine the thermal properties of an installed gage with a known heat source or to determine one thermal property when the surface heating rate is unknown during wind-tunnel tests.

Wind-Tunnel Test and Instrumentation

To demonstrate the estimation algorithm for coaxial gages further, measurements in a Mach 6 hypersonic wind tunnel will be presented for two runs of a unique test. The tunnel conditions, the model, and the instrumentation will be described.

Test conditions for the two runs (runs 14 and 15) are nearly constant except for the plate deflection angle. The Mach number is 5.85, and although stagnation temperature and pressure are nearly constant, measured time histories are used for data reduction. The constant values that will be used for computational solutions are given in Table 1 along with freestream conditions calculated assuming isentropic flow. Keyes' viscosity law[16] and a reference length just downstream of the gage of 15.24 cm are used to compute the Reynold's number.

A coaxial gage is mounted in the blunt-nosed flat plate as shown in Fig. 3. The diameter of the circular leading edge is 1.27 cm, the width of the plate is 15 cm, and the length 26 cm. The stainless-steel model has a Teflon button with a diameter of 6.35 mm and a coaxial gage with a diameter of 1.6 mm centered 14 cm from the leading edge as shown in Fig. 3. A gage is illustrated in Fig. 4 showing the surface and backface thermocouple junctions. The Teflon button is only half the length of the coaxial gage as shown. However, the change from steel to Teflon at the surface will cause a thermal mismatch because of different thermal properties.

The thermal properties used for the gage and for the steel[17] are given in Table 2. The thermal properties of the gage are lumped for chromel-constantan materials. The properties vary with temperature, and the steel properties may be in error by approximately 10% since values were extrapolated from the only data available near 300–400 K. The thermal diffusivity

Table 1 Wind-Tunnel test conditions

Run	P_o, kPa	T_o, K	P_∞, kPa	T_∞, K	R_e, x^{106}	δ, deg
14	10343	617	7.65	79	9.62	0
15	10343	617	7.65	79	9.62	0–15

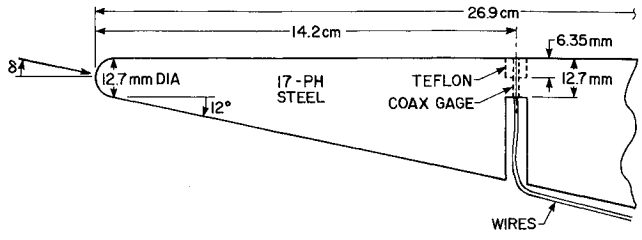

Fig. 3 Wind-tunnel model with coaxial thermocouple gage.

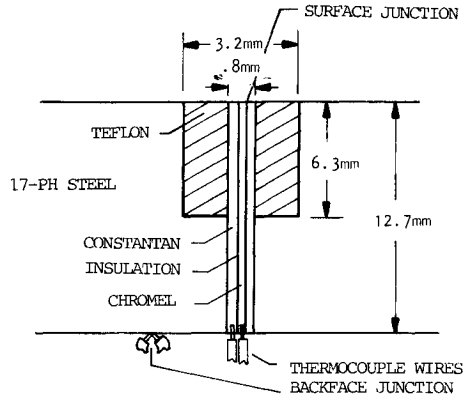

Fig. 4 Chromel-constantan coaxial thermocouple gage imbedded in steel Teflon button.

Table 2 Thermal properties

	ρ, g/cm^3	c, j/g K	K, j/cm K s	α, cm^2/s	ρcK, j/cm^2 K	ρc, j/cm^3 K
Gage	8.9	0.39	0.20	0.056	0.79	3.6
17-4 PH steel	7.7	0.27	0.10	0.049	0.46	2.1

given in Table 2 for the gage matches the diffusivity of the steel within the error of the properties, but the product ρcK [which is usually matched because of Eq. (1)] does not match well. For a good thermal match at the surface, both the diffusivity and the product ρc shown in the last column of Table 2 should be matched. This can be concluded if Eq. (4a) is investigated at the surface. Since Teflon has a lower conductivity and higher heat capacity than the steel or the coaxial gage, the Teflon button causes a thermal mismatch. This mismatch will cause the heat-transfer coefficient to vary in time.

Wind-Tunnel Results

Although the presented gage installation is not recommended for most applications, it is convenient for illustrating the unique capabilities of the estimation algorithm and exaggerates the thermal mismatch problem. The estimation algorithm is used to verify first the thermal properties and then the effective gage length. Since the test is for a longer duration than usual, the heat-transfer coefficient can be determined immediately upon injection into the wind tunnel. Although the gage installation is not thermally matched, the results for the first fraction of a second are comparable to other results with a thermally matched gage. The short- and long-duration results are therefore presented at the same time. Results for zero deflection angle (run 14) are presented first using option 2 of the new estimation algorithm and compared to the inverse algorithms for completeness. Then, results for a pitch sweep (run 15) are presented using all options. Finally, a

two-dimensional solution of the heat equation for the Teflon button and coaxial gage use the heat-transfer results as input to predict surface temperatures for the teflon, steel, and gage.

Before gaining confidence in any heat-transfer results, the thermal properties should be verified. The estimation algorithm can verify the properties and even correct them in some cases. For the coaxial gage, either the heat-transfer coefficient must be known to be constant or the backface measurement must respond significantly out of the noise level. The long duration runs presented provide a sufficient backface response. Using option 2 of the estimation algorithm for both runs 14 and 15, a factor on conductivity (ϕ_K) is estimated to be less than 0.5. Without $\phi_K = 0.5$ (i.e., $\phi_K = 1$), the estimation algorithm cannot match the backface temperature time history (the backface temperature increases by 5 K instead of the measured 1 K increase in run 14). Investigation of the thermal properties and discovery of data in Ref. 17 allowed an extrapolation of the properties to the lower operating temperatures, as given in Table 2. Thus, an error in thermal properties can be identified.

An effective gage length can also be determined using option 2 of the estimation algorithm if two- or three-dimensional effects are important. By assuming no heat flux at the backface, a factor on the effective gage length (ϕ_x) is computed for both runs 14 and 15 to be 0.8. Thus, the effective gage length is 20% longer than the actual coaxial gage. The model is also 50% thicker adjacent to the gage location as shown in Fig. 3. Thus, additional heat sink provided by the effective length is a very believable result that cannot be obtained by other algorithms.

The heat-transfer results for run 14 with the plate at zero deflection are shown in Fig. 5 for all three inverse algorithms and the estimation algorithm using option 2. All algorithms gave similar results as shown. However, the measurements are smoothed by a 10-point least-squares algorithm only for the inverse algorithms. Such smoothing is common practice, but such an arbitrary manipulation is not considered acceptable in stochastic estimation theory. The resulting heat-transfer coefficient is assumed to be smooth by the estimation algorithm, and perhaps the linear spline shown in Fig. 5 is too smooth or needs more time segments. The time variation in the heat-transfer coefficient is shown by the increase given by all algorithms. The estimation algorithm determined a time slope (h_t) that could be used to correct the heat transfer back to an isothermal wall value at tunnel injection (approximately $t = 2$ s). A short-duration test would only provide heat-transfer results for a fraction of a second, similar to the results shown. However, some heating to the plate during tunnel startup, injection of the model through the wall shear layer, and a finite injection time cause difficulties for all data reduction methods.

The heat-transfer results for run 15 with a pitch sweep provide an enormous amount of data in a single test run. Results at zero deflection after model injection can be compared with the previous run and with results after the pitch sweep to 15 deg deflection angle returns to zero deflection. However, the pitch sweep is of more interest. First, only one time slope (h_t) and five deflection slopes ($h_{\delta 1}$, $h_{\delta 2}$, ...,$h_{\delta 5}$) are computed by the estimation algorithm using option 1. The resulting heat-transfer coefficient is plotted vs deflection angle instead of time in Fig. 6. A hysteresis loop is shown during the pitch sweep, since the coefficient is higher during the pitch sweep from 0–15 deg than for the sweep from 15 deg back to 0 deg. The deflection angle time history is shown in Fig. 7 along with surface and backface temperatures. Although this type of hysteresis loop has been predicted theoretically,[2] the coefficient is expected to increase in time due to increasing leading-edge temperature and the thermal mismatch. In addition, the estimation algorithm indicated large residual errors.

Because of difficulty in reducing data for the pitch sweep in run 15, options 2 and 3 of the estimation algorithm with numerous time segments are needed. Using option 2 with three

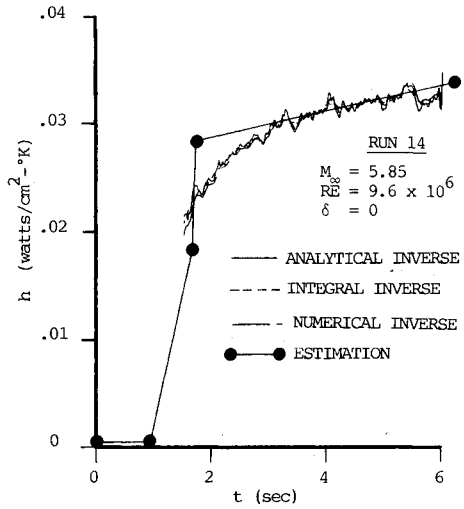

Fig. 5 Heat-transfer coefficient time history for zero deflection.

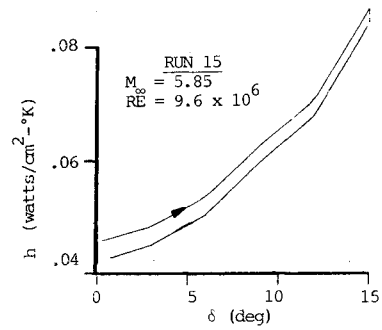

Fig. 6 Heat-transfer coefficient for pitch sweep using estimation algorithm (option 1).

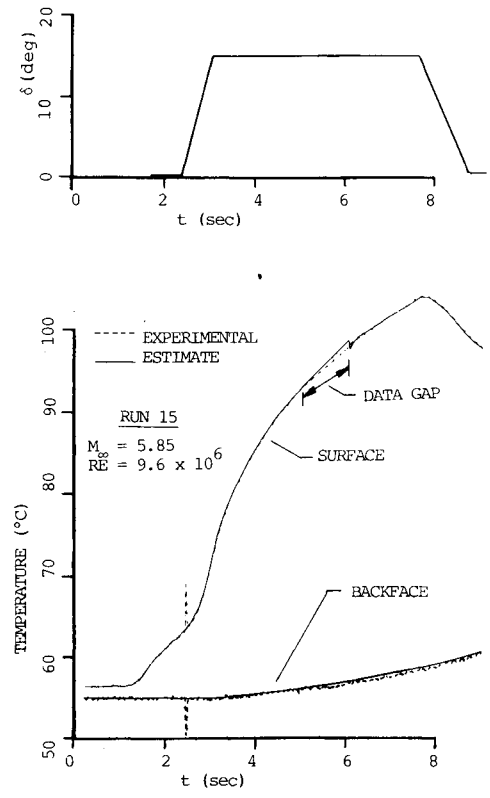

Fig. 7 Deflection/temperature time histories for pitch sweep.

time segments corresponding approximately to tunnel startup, a short time segment immediately after injection, and the pitch sweep helps the residual error problem. Increasing the number of time segments (i.e., computing h_0 and h_t repeatedly over contiguous time intervals) reduces the residual error. However, if the number of measurements in a time segment becomes small, the scoring technique used in Eq. (13) is not valid. This problem is corrected by option 3, which only estimates h_0 over each sampling interval but uses numerous measurements. The residual error is reduced, as shown in Fig. 7, by agreement between experimentally measured temperature and the estimated temperature from the algorithm. The heat-transfer coefficient using option 3 is shown in Fig. 8 vs deflection angle. Results from the inverse algorithms are also presented and are similar except for the numerical inverse algorithm. A large gap of missing data, as shown in Fig. 7, caused problems for all algorithms, expecially the numerical inverse method. The problem is illustrated better in the time history plot shown in Fig. 9. The inverse results are higher even before the data gap for reasons already discussed for the previous check cases. The decrease of the coefficient in time after $t = 4$ is also shown by all algorithms. This decrease and the associated heat-transfer coefficient magnitudes can be explained with the help of computational solutions to the heat and flow equations.

Computational Solutions of Heat and Flow Equations

The heat-transfer results from the estimation algorithm in Fig. 9 are first input to a numerical solution of the two-dimensional heat equation to determine temperatures throughout the Teflon button and coaxial gage. The maximum differences in surface temperatures are then used as wall boundary conditions for solutions of the Navier-Stokes and boundary-layer flow equations.

Temperature time histories at discrete nodes throughout the material for the coaxial gage installation are predicted using an algorithm for the solution of the two-dimensional heat equation. Differences in the surface temperatures between the steel, Teflon button, and the coaxial gage are predicted to be a maximum of 36 K if each is assumed to be isolated. However, conduction from the Teflon to the gage will increase from zero initially to a maximum and then decrease as the material temperatures increase toward thermal equilibrium. This decrease explains the decrease in the heat transfer (as well as part of the earlier increase) at constant deflection angle of

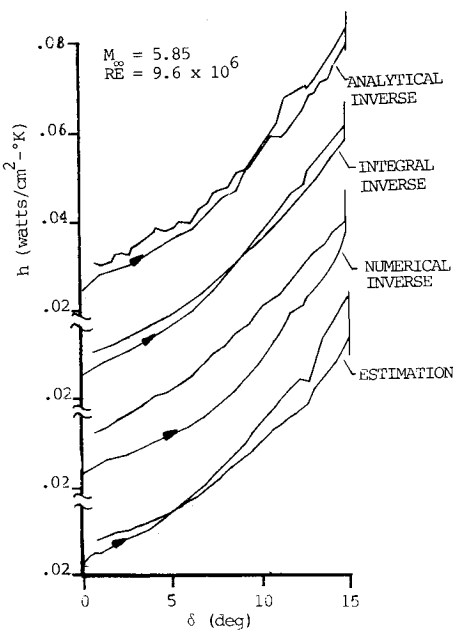

Fig. 8 Heat-transfer coefficient for pitch sweep.

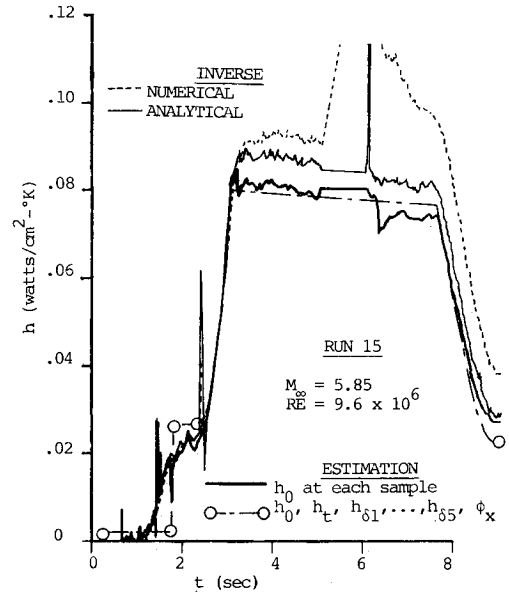

Fig. 9 Heat-transfer coefficient time history for pitch sweep.

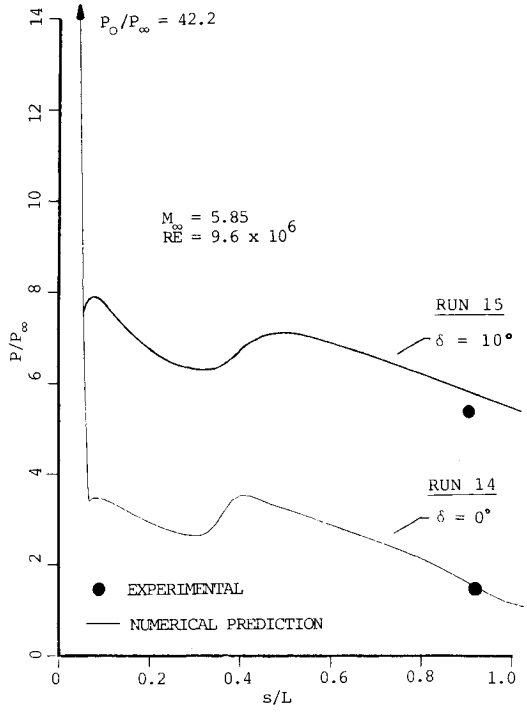

Fig. 10 Comparison of numerically predicted and measured pressures.

15 deg in Fig. 9. Therefore, increases in the heat-transfer coefficient are expected because of increasing temperatures at the leading edge, the thermal mismatch (thus temperature step), and heat conduction. For long durations, this increase will decrease, however.

Since an unsteady flow solution coupled with the wall temperature is not available, steady solutions are predicted using the maximum temperature differences from the heat equation solutions. Both explicit[18] and implicit solutions[19,20] of Navier-Stokes equations were attemped. A very fine grid near the wall is necessary for accurate heat-transfer predictions. Because of the fine grid, the explicit solution failed at the stagnation point, and the explicit shock-fitting procedure in the implicit solution diverged. A flow solution is obtained by using a coarse grid and inviscid boundary conditions in the

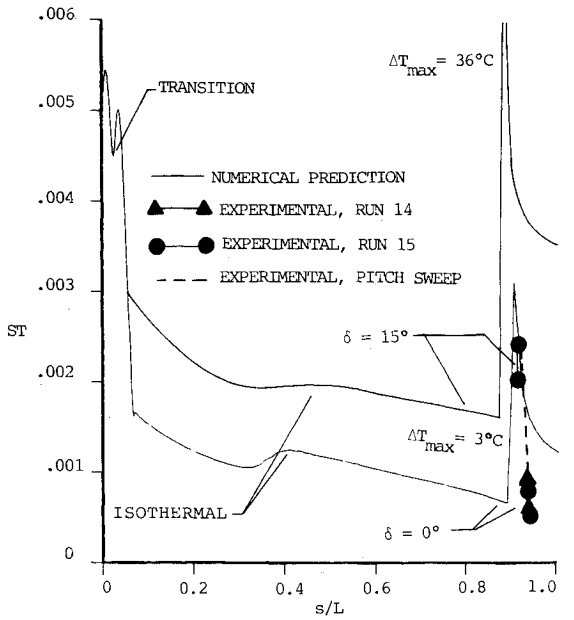

Fig. 11 Stanton number comparison of numerical predictions (with maximum thermal mismatch) and experiment.

implicit algorithm for the Navier-Stokes equations, but the heat transfer is not predicted. The predicted pressure distribution is then used in a numerical solution of the boundary-layer equations for stagnation-point heat transfer and transition to turbulent heating downstream.[21] The resulting pressure distribution from the Navier-Stokes solution is shown in Fig. 10. The predicted heat transfer is shown in terms of the Stanton number in Fig. 11 and is compared to the experimental results (runs 14 and 15) from the estimation algorithm. The experimental variations of the Stanton number (i.e., heat-transfer coefficient) are bounded by the predicted solutions with the maximum temperature differences of 36°C for $\delta = 15$ deg and 3°C for $\delta = 0$ deg. Thus, the experimental trends agree with the predicted trends.

Conclusions and Recommendations

In conclusion, a new estimation algorithm has been demonstrated using simulated and real coaxial thermocouple data. Since the correct results are known for the simulated data, unique features and characteristics of the algorithm are verified without many of the complications and uncertainties encountered with real data. Some of the unique features include determination of specific heat, conductivity, effective gage length, a "best" heat-transfer coefficient, and time variations in the heat-transfer coefficient. Some of these features are used with wind-tunnel data, and changes in heat transfer due to deflection angle separated from changes in time due to a thermal mismatch. Trends for the time variations are verified by comparing with inverse algorithms and numerical flow solutions. However, features exceeding those of other algorithms are verified, but can always be enhanced further.

As a result of this investigation, recommendations concerning gage installation are needed to enhance application of an estimation algorithm as follows:

1) Account for tangential conduction by using a very short gage length and model skin thickness, preferably with the same thickness as the model (another measurement near the surface would be an alternative).

2) Determine the surface coating thickness or depth according to the fastest response needed; thus, sampling requirements are minimized and noise is better distinguished from transient variations by the estimation algorithm, if the measurement is at the second node.

3) Thermally and chemically match the gage at the surface with the surrounding material, and make it as small as possible (such that thermal capacity is negligible).

4) Pulse the installed gage with a known heat source with the precise pulse initiation time known, and estimate the specific heat capacity, conductivity, and effective gage length at several heating levels since the properties vary with temperature.

5) Provide a fast deflection sweep in a convective heating environment for thermal property estimation, but use a slower sweep rate for better resolution of heat transfer at intermediate deflection angles.

With these recommendations and the estimation algorithm, the accuracy of heat-transfer measurements should improve, and test duration should increase to allow more transient testing using pitch sweeps.

Acknowledgments

Thanks to W. C. Ragsdale of the Naval Surface Weapons Center and Professor J. E. Hitchcock of the Air Force Institute of Technology for help with the inverse algorithms.

References

[1]Hodge, J.K., Woo, Y.K., and Cappelano, P.T., "Parameter Estimation for Imbedded Thermocouples in Space Shuttle Wind Tunnel Test Articles with a Nonisothermal Wall," AIAA Paper 83-1533, June 1983.

[2]Lange, K.J., "Unsteady Solution of the Boundary Layer Equations with Application to Space Shuttle Tiles," M.S. Thesis, Air Force Institute of Technology, Wright-Patterson AFB, OH, GAE/AA/84D-11, June 1985.

[3]Chung, P.M., Liu, S.W., and Mirels, H., "Effect of Discontinuity of Surface Catalycity on Boundary Layer Flow of Dissociated Gas," *International Journal of Heat and Mass Transfer*, Vol. 6, 1963, pp. 193-210.

[4]McCarty, R.L. and Hodge, J.K., "Nonequilibrium Parabolized Navier-Stokes Solution Over a Noncatalytic-Catalytic Discontinuity," Air Force Institute of Technology, TR (to be published).

[5]Knox, E.C. and Martindale, W.R., "Coax Heat Transfer Gage Usage in the VKF Tunnels B and C," VKF-TM-B.6, 1979.

[6]Jordan, J.L. and Kessel, P.L., "Heat Transfer Rate Measurements Obtained in a Highly Erosive Two-Phase Flow Field," AIAA Paper 83-0584, Jan. 1983.

[7]Neumann, R.D. and Hayes, J.R., "Advanced Techniques for the Acquisition of Aerodynamic Heating Data in Hypersonic Continuous Flow Test Facilities," 3rd Aerothermal Workshop, Snowmass, CO, June 1984.

[8]Cahoon, N.T., "Heating Parameter Estimation Using Coaxial Thermocouple Gages in Wind Tunnel Test Articles," M.S. Thesis, Air Force Institute of Technology, Wright-Patterson AFB, OH, GAE/AA/84D-3(ADA154467), 1984.

[9]Cook, W.J. and Felderman, E.J., "Reduction of Data from Thin Film Heat-Transfer Gages: A Concise Numerical Technique," *AIAA Journal*, Vol. 4, March 1966, pp. 561-562.

[10]Hodge, J.K. and Audley, D.R., "Aerothermodynamic Parameter Estimation From Space Shuttle Thermocouple Data During Transient Flight Test Maneuvers," AIAA Paper 83-0482, Jan. 1983; also *Journal of Spacecraft and Rockets*, Vol. 23, Sept.-Oct. 1986, pp. 453-460.

[11]Lutes, C.D. and Hodge, J.K., "Nonlinear Modelling and Initial Condition Estimation for Identifying the Aerothermodynamic Environment of the Space Shuttle Orbiter," AIAA Paper 84-1749, June 1984.

[12]Beck, J.V., Blackwell, B., and St. Clair, C.R., Jr., *Inverse Heat Conduction, Ill-Posed Problems*, Wiley-Interscience, New York, 1985, pp. 1-19.

[13]Kendall, D.N. and Dixon, W.P., "Heat Transfer Measurements in a Hot Shot Wind Tunnel," IEEE Aerospace Systems Conference, Seattle, WA, July 1966.

[14]Sagsteter, P.W., "Numerical Computation of the Matrix Ricatti Equation for Heat Propagation During Space Shuttle Reentry," M.S. Thesis, Air Force Institute of Technology, Wright-Patterson AFB, OH, GCS/MA/82D-7, 1982.

[15]Maybeck, P.S., *Stochastic Models, Estimation and Control*, Vols. 2 and 3, Academic Press, New York, 1982.

[16]Keyes, F.G., "A Summary of Viscosity and Heat Conduction

Data for He, A, H, CO, CO2, H2O, and Air," *Transactions of ASME*, Vol. 73, 1951, pp. 589–596.

[17]*Thermophysical Properties of Matter,* The TPRC Data Series, Vols. 1 and 4, edited by Y.S., Touloukian, Purdue Research Foundation, 1970.

[18]Shang, J.S., Bunning, P.G., and Hankey, W.L., "Performance of a Vectorized Three-Dimensional Navier-Stokes Code on a CRAY-1 Computer," *AIAA Journal*, Vol. 18, Sept. 1980, pp. 1073–1079.

[19]MacCormack, R.W., "Current Status of Numerical Solutions of the Navier-Stokes Equations," AIAA Paper 85-0032, Jan. 1985.

[20]Scherr, S. and Shang, J., "Flows Over Blunt Bodies Using a Flux-Splitting and Shock-Fitting Scheme," AIAA Paper 86-0340, Jan. 1986.

[21]Shang, J.S., Hankey, W.L., and Dwoyer, D.L., "Numerical Analysis of Eddy Viscosity Models in Supersonic Turbulent Boundary Layers," *AIAA Journal*, Vol. 11, 1973, pp. 1677–1683.